Journal of Nuclear Materials 376 (2008) 222–228

Contents lists available at ScienceDirect

Journal of Nuclear Materials

journal homepage: www.elsevier.com/locate/jnucmat

Positron annihilation characteristics of ODS and non-ODS EUROFER isochronally annealed

Y. Ortega *, V. de Castro, M.A. Monge, A. Muñoz, T. Leguey, R. Pareja

Departamento de Física, Universidad Carlos III de Madrid, 28911 Leganés, Spain

ARTICLE INFO

Article history:
Received 25 January 2008
Accepted 3 March 2008

PACS:
28.52.Fa
78.70.Bj
68.37.Lp

ABSTRACT

Yttrium oxide dispersion strengthened (ODS) and non-ODS EUROFER produced by mechanical alloying and hot isostatic pressing have been subjected to isochronal annealing up to 1523 K, and the evolution of the open-volume defects and their thermal stability have been investigated using positron lifetime and coincidence Doppler broadening (CDB) techniques. Transmission electron microscopy (TEM) observations have also been performed on the studied samples to verify the characteristics of the surviving defects after annealing at 1523 K. The CDB spectra of ODS EUROFER exhibit a characteristic signature that is attributed to positron annihilation in Ar-decorated cavities at the oxide particle/matrix interfaces. The variation of the positron annihilation parameters with the annealing temperature shows three stages: up to 623 K, between 823 and 1323 K, and above 1323 K. Three-dimensional vacancy clusters, or voids, are detected in either materials in as-HIPed condition and after annealing at $T \leqslant 623$ K. In the temperature range 823–1323 K, these voids' growth and nucleation and the growth of other new species of voids take place. Above 1323 K, some unstable cavities start to anneal out, and cavities associated to oxide particles and other small precipitates survive to annealing at 1523 K. The TEM observations and the positron annihilation results indicate that these cavities should be decorated with Ar atoms absorbed during the mechanical alloying process.

1. Introduction

Reduced activation ferritic martesitic (RAFM) and oxide dispersion strengthened (ODS) steels are considered as promising structural materials for the future fusion reactors because of their creep strength and swelling resistance [1–4]. The ODS steels, produced by mechanical alloying (MA) and consolidation by hot extrusion or hot isostatic pressing (HIP) have been developed, and their mechanical properties and microstructure features extensively investigated [3–8]. However, ODS materials produced by MA exhibit poor impact properties and a high ductile-brittle transition temperature (DBTT) [5,8–10]. These particular characteristics will limit the performance of the ODS steels in a fusion reactor. The origin of these adverse characteristics is attributed to excess oxygen introduced by MA, residual porosity, or nanovoids, present in the consolidated material, and carbide precipitation biased by the high density of structural defects still present after the HIP treatment. These structural defects also appear to be related to the swelling resistance that has been found in ODS steels. The low accumulation rate of irradiation-induced defects in these materials has been attributed to point defect sinks associated to either the oxide particles or the oxide/matrix interfaces, as well as to grain boundaries and laths [7,11]. These sinks also appear to be H, He and Ar traps [12–14], and therefore they would be open-volume defects.

Positron annihilation spectroscopy (PAS) is a very powerful technique to investigate open-volume defects in metals because these defects are strong traps for thermal positrons in the crystal lattice. This technique has been applied to study irradiation damage in steels used in nuclear technology [15,16]. In addition to the positron lifetime measurements, which give information about the size of the positron traps, coincidence Doppler broadening (CDB) measurements of the annihilation radiation can reveal the chemical environment of the traps [17]. Thus, concurrent positron lifetime and CDB measurements in ODS and non-ODS steels can contribute to elucidate the nature, localization and thermal stability of the defects responsible for the swelling resistance and detrimental effects on the mechanical properties. The present work reports positron annihilation experiments and transmission electron microscopy (TEM) studies performed on the reduced activation 9CrWVTa steel EUROFER 97, ODS and non-ODS, in order to achieve more understanding about the role of the oxide particles and the structural defects in the properties of the ODS steels.

* Corresponding author.
E-mail address: yanicet@fis.ucm.es (Y. Ortega).

0022-3115/$ - see front matter © 2008 Elsevier B.V. All rights reserved.
doi:10.1016/j.jnucmat.2008.03.005

2. Experimental

2.1. Materials

Gas-atomised EUROFER 97 powder (Studsvid, Sweden) with particle sizes <45 μm was milled with 0.25 wt% Y_2O_3 for 24 h under a pure Ar atmosphere in a horizontal attritor. Details of the milling procedure and the characteristics of the milled powder are reported elsewhere [18]. Y_2O_3-free EUROFER powder was also milled under identical conditions. For comparative experiments, milled Y_2O_3/EUROFER powder, and un-milled and milled Y_2O_3-free powders were canned and degassed at 673 K for 24 h in vacuum, and then the cans sealed. These materials after consolidation were labeled by ODS, UM and M, respectively. The powders were consolidated by HIP at 1373 K for 2 h under a pressure of 198 MPa. During cooling above the M_s temperature (~650 K), the temperature went down exponentially at rates >30 K/min while the pressure descended linearly with temperature. The densities measured in a He pycnometer resulted in (7.76 ± 0.06) g/cm^3 for ODS EUROFER, and (7.77 ± 0.03) and (7.79 ± 0.02) g/cm^3 for un-milled (UM) and milled (M) EUROFER, respectively, compared to a theoretical density of 7.82 g/cm^3. A pair of samples cut from a plate of original EUROFER 97 fabricated by Böhler AG (Austria) was used as reference. In addition, samples of Y and Y_2O_3, suitably prepared, were measured by CDB for comparison. The Y_2O_3 samples were produced by cold compaction from the same Y_2O_3 nano-powder used to prepare ODS EUROFER.

2.2. PAS experiments

Positron annihilation experiments were performed on the pairs of samples 10 × 10 × 1 mm^3, cut from each consolidated ingots, in as-HIP state and after isochronal annealing. The samples were annealed for 90 min up to 1523 K in 100 K steps in a vacuum of <10^{-6} Pa. Experiments in parallel were also made with a pair of samples of original EUROFER 97.

CDB measurements were carried out using two HP Ge detectors in timing coincidence, placed face to face and separated by 40 cm from each other. The pair of samples, enclosing a ^{22}Na positron source, was positioned just at the half-way point between the detectors. The pulses from each detector were connected to an ORTEC-572 amplifier with a shaping time of 2 μs. The gain of each amplifier was adjusted to have exactly the same calibration factor for both detectors (~81.1 eV/channel). Signals from the amplifiers were fed into a two-dimensional multichannel analyzer (2D-MCA). Two analogue-digital converters were used with a conversion range of 16 K, and the 2D-MCA was adjusted to focus the annihilation peak corresponding to 511 keV at the center of a 512 × 512 matrix. The analyzed CDB spectra were cumulative spectra formed by the addition of twenty spectra that did not exhibit electronic drift, each with more than 10^6 counts in the 512 × 512 coincidence matrix. The cumulative spectra had 1×10^7 counts in the strip centered on the matrix diagonal that fulfilled the condition $2m_0c^2 - 1.6\ \text{keV} < E_1 + E_2 < 2m_0c^2 + 1.6\ \text{keV}$; here E_1 and E_2 denote the energies of the annihilating gamma-ray pairs, m_0 the electron rest mass and c the light speed. To emphasize the difference between the CDB spectra, the intensity is normalized by dividing the counts at a given γ energy by the corresponding for the reference samples of EUROFER. Previously, the areas under the CDB spectra were normalized to unity and smoothed.

Positron lifetime measurements were performed with a conventional fast-fast coincidence spectrometer equipped with two NE111 plastic scintillators. The time resolution of the system, measured for ^{22}Na energy settings, was 240 ps (FWHM). The time resolution and the contribution of the positron source to the lifetime spectrum were determined from measurements on references samples and analyses using the program RESOLUTION. The lifetime spectra were analysed using the program POSITRONFIT.

2.3. Tem

TEM observations were performed on the same pairs of samples used in the PAS experiments, after annealing at 1523 K. Three millimeter discs punched from the thinned samples were electropolished at 243 K and 20 kV in an electrolyte solution of 5% $HClO_4$ + 95%CH_3OH. The observations were carried out in a Philips CM20 at 200 kV equipped with energy dispersive X-ray spectrometer (EDS).

3. Results

3.1. Positron lifetime measurements

After subtracting the positron source contribution, base EUROFER and UM EUROFER exhibited a single-component lifetime spectrum after annealing through the whole temperature range. The spectra were characterised by a lifetime that varied between 140 and 155 ps for base EUROFER, and between 143 and 152 ps for UM EUROFER, irrespective of the annealing temperature, as shown in Fig. 1.

The lifetime spectra for ODS- and M-EUROFER were properly fitted to a sum of two exponential components, and characterised by a mean positron lifetime defined by $\bar{\tau} = I_1\tau_1 + I_2\tau_2$, where τ and I represent the lifetime and relative intensity of the spectral component, respectively. Fig. 1 shows the $\bar{\tau}$ values as a function of annealing temperature for both materials. It was found that $\bar{\tau}$ increases after annealing above 823 K in these two materials. For ODS EUROFER, $\bar{\tau}$ increases continuously from a value of ~187 ps to 227 ps after annealing at 1523 K; for M-EUROFER, the $\bar{\tau}$ value goes up from ~160 ps up to a maximum value of ~205 ps after annealing at 1323 K, and decreases for annealing above 1323 K.

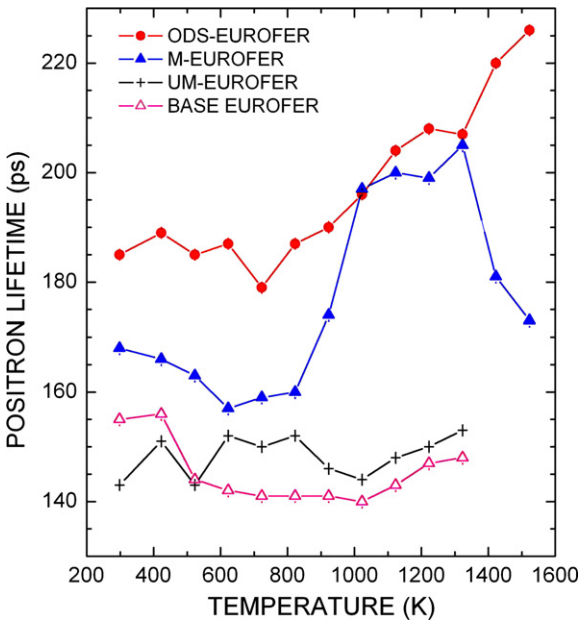

Fig. 1. Positron lifetime for base, un-milled-(UM), milled-(M) and ODS-EUROFER as a function of annealing temperature. The values for base- and UM-EUROFER correspond to single lifetime values and those for M- and ODS-EUROFER are mean lifetime values.

The τ_1 and τ_2 values, and the intensity I_2 of the second lifetime component, are represented versus annealing temperature in Figs. 2 and 3, respectively. The experimental spectra were well fitted assuming two-component spectra, but the parameters obtained from these analyses are inconsistent with the assumed two-stage trapping model; three-component analyses yielded unrealistic parameters. A well-defined behaviour of the parameters obtained from the two-component analyses is not observed because various types of defects having close lifetime values may contribute to each component of lifetime spectra.

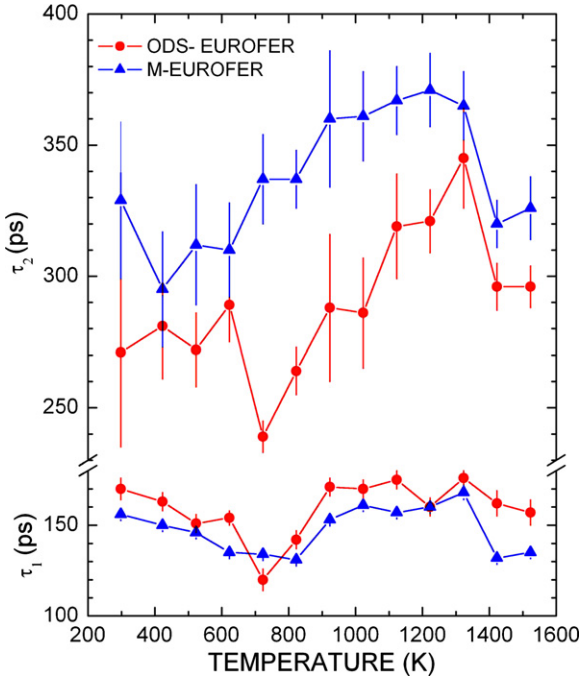

Fig. 2. Lifetime values τ_1 and τ_2 for milled-(M) and ODS-EUROFER as a function of annealing temperature.

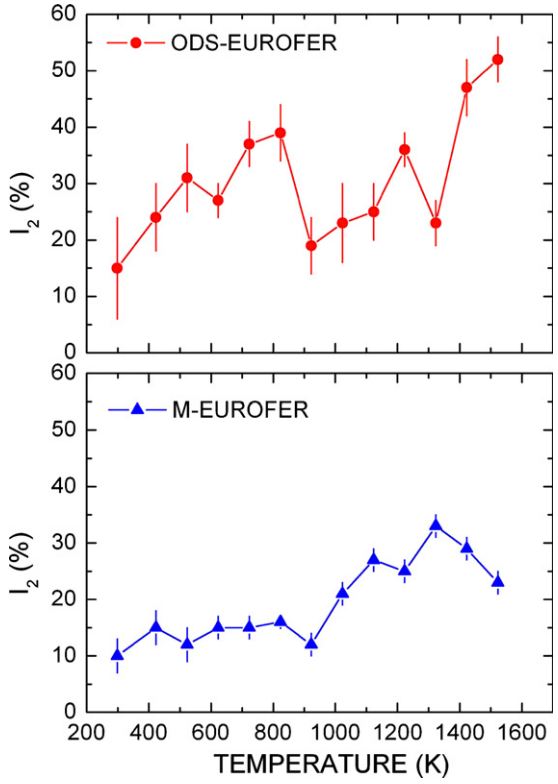

Fig. 3. Intensity I_2 of the second lifetime component for milled-(M) and ODS-EUROFER as a function of annealing temperature.

3.2. CDB measurements

Figs. 4 and 5 show the CDB ratio spectra for pure Fe, Y and Y_2O_3, and for the materials in the as-HIPed condition, respectively; the spectra are normalised to the base EUROFER spectrum. The high concentration of Cr in the EUROFER materials is responsible for the depletion in the high-momentum region, compared to the Fe CDB spectrum. This is the expected effect for Cr in a Fe matrix [19]. It is also observed that the three EUROFER materials in the as-HIPed condition present less annihilation events with core electron of high momentum than the base EUROFER, as Fig. 5 reveals. The spectra for the non-ODS materials, i.e. for UM- and M-EUROFER, are alike and qualitatively different from the one for ODS EUROFER. The discrepancies become more evident increasing the annealing temperature as Figs. 6 and 7 show. In particular, after annealing at $T \geqslant 1123$ K it is clear that the shape of the curves for ODS EUROFER is equal to that for Y_2O_3 in the high momentum range ($p_L \geqslant 15 \times 10^{-3}\ m_0c$), and the differences with the reference spectrum increase.

Also, annealing induces significant changes in CDB spectra of the non-ODS materials. The contribution of high momentum electrons in UM EUROFER increases related to M EUROFER with the annealing temperature until it becomes similar to the one for base EUROFER after annealing at 1123 K. The annealing effect on the ratio spectrum of M EUROFER is different as Fig. 8 shows. Its momentum distribution trends to match to that for the reference EUROFER for annealing at 723 K, apparently. Afterwards, the contribution from high momentum electrons descends significantly and the one from low momentum electrons increases for annealing above 1123 K. Finally, the momentum distribution trends once again to match to the reference one after annealing above 1523 K. It should

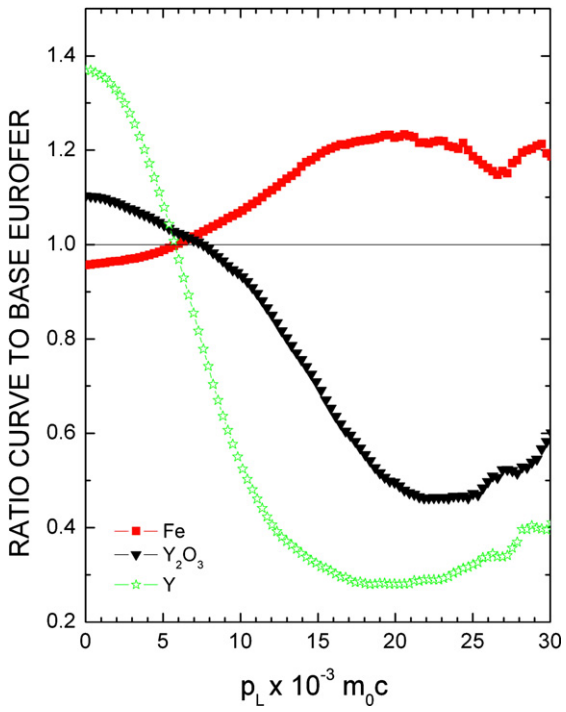

Fig. 4. CDB ratio spectra for pure Fe, Y and Y_2O_3.

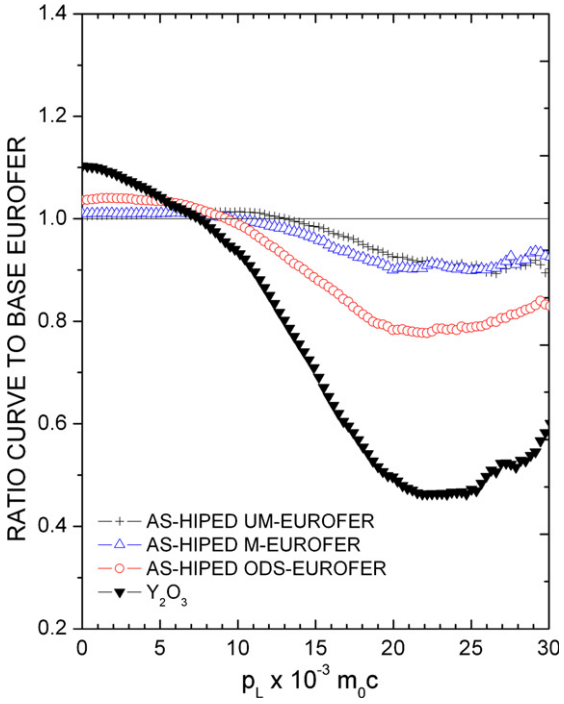

Fig. 5. CDB ratio spectra for un-milled-(UM), milled-(M) and ODS-EUROFER in the as-HIPed condition. The CBD ratio spectrum for pure Y_2O_3 is shown for comparing.

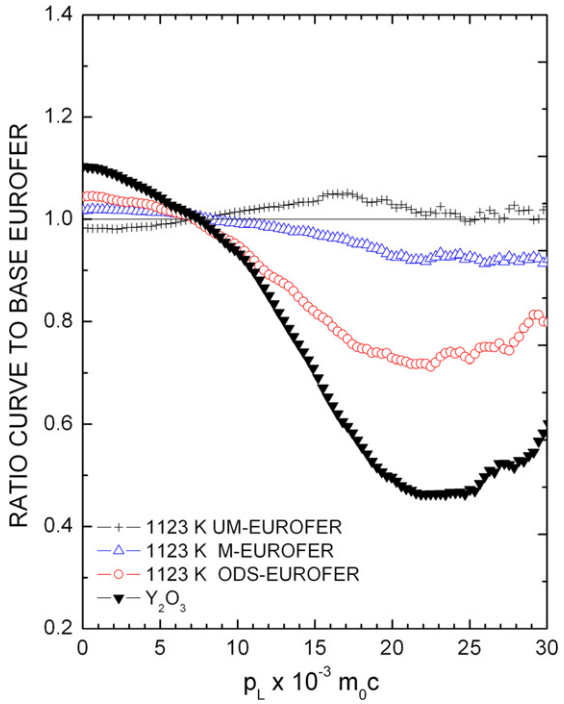

Fig. 6. CDB ratio spectra for un-milled-(UM), milled-(M) and ODS-EUROFER after annealing at 1123 K. The CBD ratio spectrum for pure Y_2O_3 is shown for comparing.

be noted that the variation of the mean positron lifetime for M-EUROFER, shown in Fig. 1, also reflects behaviour similar to the one described above. This shows the reliability and consistency of the results.

3.3. Tem

Through-focal observations, performed on samples of ODS- and M-EUROFER after the final anneal at 1523 K, revealed the presence

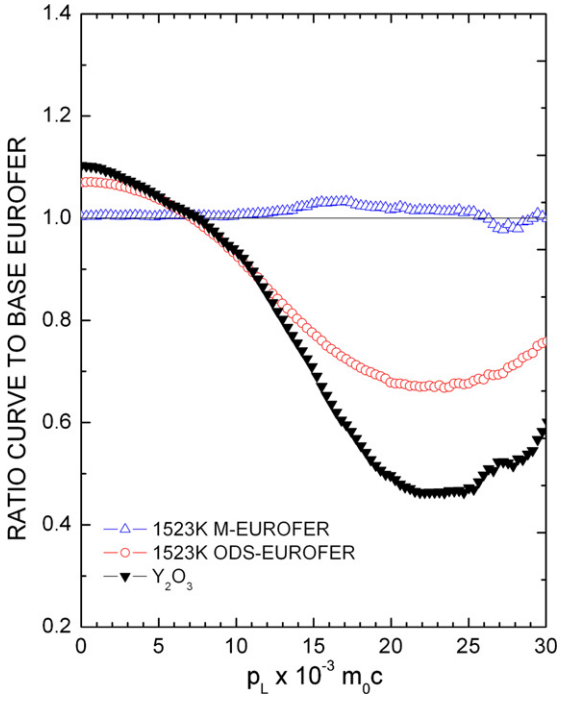

Fig. 7. CDB ratio spectra for milled-(M) and ODS-EUROFER after annealing at 15-23 K. The CBD ratio spectrum for pure Y_2O_3 is shown for comparing.

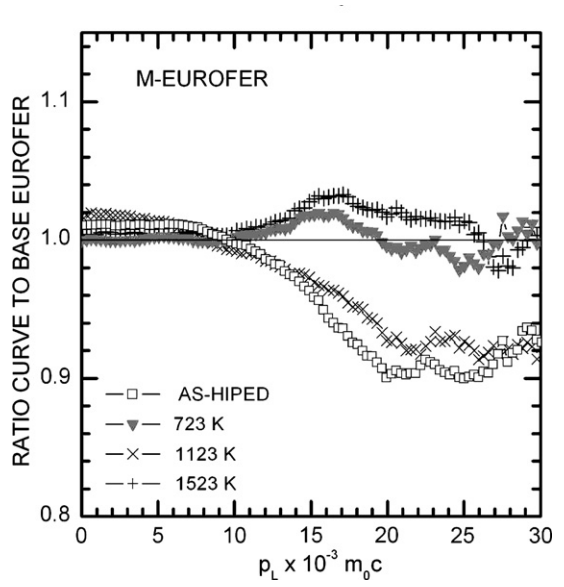

Fig. 8. Positron lifetime for base, un-milled (UM), milled-(M) and ODS-EUROFER as a function of annealing temperature.

of voids with sizes up to ~25 nm as Figs. 9 and 10 show. These nanovoids are located on grain boundaries, dislocations and randomly in the matrix. Moreover, in the case of ODS EUROFER the EDS and selection area electron diffraction analyses revealed that the cavities are mostly associated to the Y_2O_3 nanoparticles. These cavities exhibit contrast characteristics similar to the ones corresponding to Ar-decorated cavities in an ODS-9CrWVTaTi steel mechanically alloyed with 0.5 wt% of Y_2O_3 and Ti, reported previously [14]. Unfortunately, energy-filtered (EF) TEM imaging and electron energy spectroscopy (EELS) could not be done at present to confirm the presence of trapped Ar in these cavities. In M EUROFER nanovoids are mainly found associated to very small particles. These particles have not been identified.

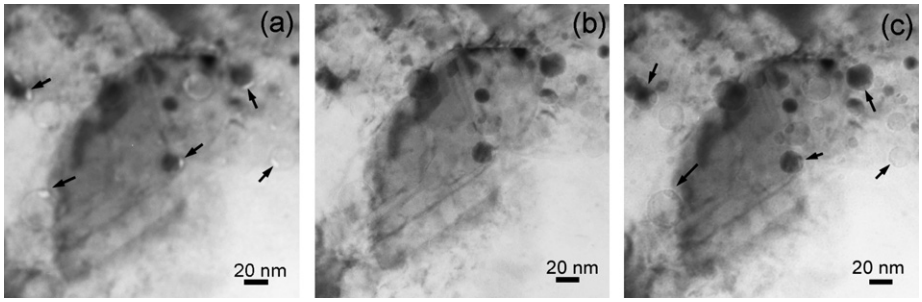

Fig. 9. TEM through-focal images of voids (arrowed) located next to small Y_2O_3 particles in ODS EUROFER annealed at 1523 K. (a) Under-focused by 1 μm, voids appear as white dots surrounded by a dark Fresnel fringe; (b) in-focus, voids show almost no contrast; (c) over-focused by 1 μm, voids appear as black dots surrounded by a bright Fresnel fringe.

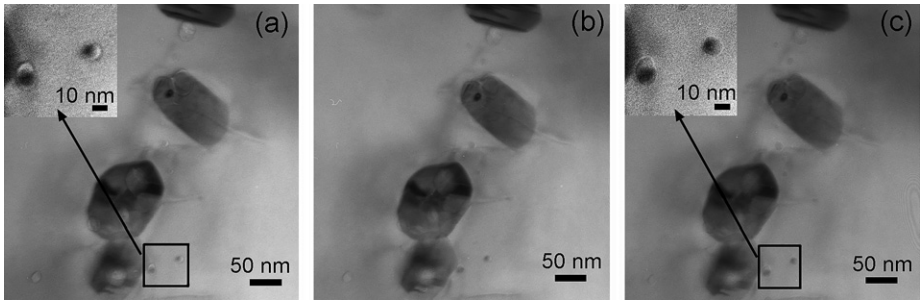

Fig. 10. TEM through-focal images of voids in M EUROFER annealed at 1523 K. Some of the voids (arrowed) are found associated to small unidentified precipitates. (a) Under-focused by 1 μm, (b) in-focus, (c) over-focused by 1 μm.

4. Discussion

HIPed UM EUROFER and base EUROFER yield single positron lifetime values that are longer than the bulk lifetime for α-Fe (110 ps) and vary in the value range of the characteristic lifetimes for annealed steels, ~140 ps, and a value significantly lesser than that attributed to dislocations in iron and steels, ~165 ps [20,21]. The microstructure of these materials is very complex with a high density of dislocation and different types of carbide precipitates, as the TEM observations confirm, and it is impossible to discriminate which positron traps control the observed positron lifetime in these two materials. The positron lifetime value for carbide precipitates that can be formed in steels is expected to be similar to the bulk lifetime for α-Fe [15]. Thus, the observed variation of the single positron lifetime and the CDB ratio spectrum is attributed to annealing-induced changes in dislocations and carbide precipitates present in these materials.

Either of the milled materials, ODS and non-ODS, exhibit very different behaviours with respect to the above un-milled materials. The presence of a long-lived lifetime component, τ_2, ranging between 300 and 370 ps in M-EUROFER, and between 240 and 340 ps in ODS EUROFER, indicate the formation of open volume defects such as three-dimensional vacancy clusters, i.e. small voids or cavities. However, the lifetime values and relative intensities of the lifetime components are not consistent with the two-state trapping model assuming a bulk positron lifetime similar to that for α-Fe (~110 ps) [20]. This means that there is more than one type of defect acting as positron traps in the milled materials. The first lifetime component in these materials should be attributed to annihilation events in the bulk and structural defects like carbide precipitates, grain boundaries, dislocations, vacancy-impurity complex defects associated to carbide/matrix interfaces, etc. According to theoretical calculi [22], the lifetime for positron trapped in three-dimensional vacancy clusters containing between 3 and 15 vacancies in α-Fe ranges from 232 and 386 ps. Thus, the second lifetime component would be in principle attributed to positrons trapped by three-dimensional vacancy clusters, or nanovoids, according to theoretical and experimental results in α-Fe [20,22]. The I_2 values of 10% and 15% for as-HIPed M- and ODS-EUROFER, respectively, indicate the presence of a high density of three-dimensional vacancy clusters. The TEM observations in these materials confirm the presence of these defects after annealing at 1523 K. Since a lifetime component attributable to this type of defects has not been found in the un-milled material, in as-HIPed condition and after annealing, the nanovoids in as-HIPed M- and ODS-EUROFER have to form during the HIP process due to the high density of structural defects created by the milling process.

Apparently, the CDB results are not consistent with the above conclusions because they do not reflect the expected increase in the region of the low-momentum attributable to annihilation with low-momentum electrons, i.e. with valence electrons, when positrons are trapped at vacancy-like defects. Nevertheless, if the three-dimensional vacancy clusters, i.e. voids or cavities, contain trapped gas atoms, the positron lifetime and the momentum distribution of the annihilation positron–electron pairs is quite different depending on the amount of gas atoms contained in it. Voids with trapped gas atoms have a high density of high-momentum electrons at their centre relative to a gas-free void. Thus, positrons in voids containing gas atoms sample sites of higher electron density and electrons with a higher momentum than in gas-free voids. Therefore, if the gas content is high, the momentum distribution of the annihilation pairs at the traps would be affected by the core electrons of the gas atom, that is, the low-momentum contribution due to valence electrons of the matrix would decrease and high-momentum contribution increase, together with the positron lifetime at the voids. The above is supported by theoretical calculations [22,23] and experimental results [24]. This explains why the CDB ratio curves for milled EUROFER, ODS or non-ODS, do not exhibit an enhanced low-momentum contribution in spite of

the evidence of positron trapping revealed by the positron lifetime measurements. The results for M EUROFER illustrate this situation. After annealing at 1123 K when $\bar{\tau}$ and I_2 attain the high values, i.e. when the positron trapping compared to the reference samples is higher, CDB ratio spectrum exhibits a minor enhancement of the low-momentum annihilations with valence electrons and a significant depletion in the annihilations with core electrons of high momentum, compared to base EUROFER. After annealing at 1523 K, the positron trapping in M EUROFER is still important, $I_2 = 23\%$ and $\bar{\tau} = 173$ ps, compared to trapping in base EUROFER, $\tau = 155$ ps, but its CDB spectrum matches to the reference in the low-momentum region, and exceed it slightly in the high momentum region, see Fig. 8. The above means that positrons at the voids present in M-EUROFER annealed at 1523 K have a higher probability to annihilate with electrons of high momentum than in the case of trapping at the defects present in the base EUROFER. This is interpreted as evidence of impurity trapping by the voids, very likely Ar coming from the milling process as reported elsewhere [14].

The shape likeness between the high-momentum regions ($p_L \geqslant 15 \times 10^{-3}\ m_0c$) of the CDB ratio spectra of ODS EUROFER and the one for Y_2O_3 discloses the effect of the Y_2O_3 dispersion on the positron trapping characteristics of this type of steel. Calculations for positrons in inert-gas bubbles in metals have shown that positrons are trapped at the bubbles surface, i.e. at the gas/matrix interface, and the corresponding positron lifetime τ given by [25]

$$\tau = (\lambda_{\text{surf}} + \lambda_{\text{gas}})^{-1} \quad (1)$$

where λ_{surf} represents the annihilation rate of the surface states for positron at the bare surface of the host metal, and λ_{gas} the annihilation rate with gas atoms. Experimental results for He in Al, and Kr in Cu, are consistent with the model used for the mentioned calculations. Then, if this model is extrapolated to the present experiments one would expect that the CDB spectrum shows signs of the contribution of the matrix surface to the annihilation of the positrons trapped at the gas/matrix interfaces. This idea is consistent with the CDB results that evidence positron trapping at Y_2O_3/cavity interfaces in ODS EUROFER and not in M EUROFER. It has to point out that Y has a very high positron affinity, 5.31 eV against 3.84 eV for Fe [26]. This can explain that the contribution of Y_2O_3 surface inhibits the possible contribution of the metal matrix surface.

These results agree with the TEM observations, and the evidence that the oxide particle/matrix interfaces act as strong sinks for vacancies and Ar atoms providing very favourable sites for the clustering of vacancies and gas impurities.

TEM observations after annealing at 1523 K confirmed the presence of a high density of nanovoids in M- and ODS-EUROFER, very likely containing Ar. In the case of ODS EUROFER, these nanovoids were very frequently bound with Y_2O_3 particle/matrix interfaces, see Fig. 9.

The behaviour of the parameters $\bar{\tau}$, τ_1, τ_2 and I_2 for M- and ODS-EUROFER, shown in Figs. 1–3, suggests that three main stages take place during isochronal annealing up to 1523 K.

4.1. Stage up to 623 K

Over the temperature range 300–623 K, the lifetime of the first component τ_1, due to some structural defects retained in as-HIPed M EUROFER, appears to become shorter. This would induce the observed changes in $\bar{\tau}$ and in the CDB spectrum without any significant change in the parameter corresponding to the second positron lifetime. This means that if the anneals in this temperature range produce vacancy release from these structural defects, they recombine and do not agglomerate at sinks such as the ones responsible for the second lifetime component, since the changes in the intensity I_2 and lifetime τ_2 are not significant. In the case of ODS EUROFER, these anneals produce an important increase of I_2 and a reduction of τ_1 value without significant changes in the lifetimes $\bar{\tau}$ and τ_2. This indicates that the vacancies released by the defects contributing to the short lifetime component diffuse toward sinks and give rise to new three-dimensional vacancy clusters (voids) instead of recombining. Since the oxide dispersion is what makes these materials different from each other, the Y_2O_3 particles appear to be the vacancy sinks, more specifically, the Y_2O_3/matrix interfaces as the TEM observations after annealing at 1523 K confirm.

4.2. Stage between 823 and 1323 K

In this temperature range, $\bar{\tau}$ and τ_2 increase continuously indicating the coarsening of the three-dimensional vacancy clusters responsible for the second lifetime component. Moreover, these increases in M EUROFER are followed by a remarkable increase in I_2, from ~15% to 33%, which means an enhancement of the trapping rate. The fact that τ_2 starts to increase before I_2 can be interpreted in terms of the initial coarsening of the previous vacancy clusters responsible for the second lifetime component. This process would be the result of the diffusion of vacancies, released by impurities and defects, towards these clusters after which annealing below 823 K has lowered the concentration of competitive point defects sinks such as dislocations and dislocation loops. Then, I_2 goes up for annealing at $T \geqslant 1023$ K. This lag in the I_2 increase may be attributed to the nucleation of new vacancy sinks different from those existing before. The small particles that appear associated to the cavities surviving to annealing at 1523 K in M EUROFER may have precipitated during annealing in this temperature interval.

ODS EUROFER in this temperature range exhibits a continuous increase in $\bar{\tau}$ and τ_2 but an undefined or erratic behaviour for I_2. The last may be due to the fact that there exists more than one species of competitive positron traps contributing to the second lifetime component, and thus the observed τ_2 values actually correspond to a weighted average positron lifetime for the three-dimensional vacancies clusters present in ODS-EUROFER. A simultaneous coarsening or transformation of some cluster species, and the nucleation and subsequent growth of new trap species with different cross section for positron trapping, can lead to the observed behaviour for I_2. Like in M EUROFER, the precipitation processes in this temperature range can provide the nucleation sites for the new traps.

4.3. Stage above 1323 K

The clear recovery onset of the parameters $\bar{\tau}$, τ_1, τ_2 and I_2 in M EUROFER 1323 K is the evidence for the disappearance of unstable cavities at $T \geqslant 1323$ K. Nevertheless, a high concentration of cavities still remain after annealing at 1523 K as the high I_2 and τ_2 values show and the TEM observation confirms. The fact that τ_2 drops from 370 ps to 320 ps and the CDB spectra for $T \geqslant 1323$ K do not exhibit enhanced annihilation with low-momentum electrons is the evidence for the presence of gas atom in the surviving cavities. Gas-free voids and very small gas-vacancy clusters, isolated in the matrix, i.e. not associated to particles, would be the unstable voids annealing out at $T \leqslant 1323$ K. It should be mentioned that TEM observations in samples in as-HIPed conditions or annealed at $T \leqslant 1323$ K to reveal the presence of these small voids and particles are actually unfeasible because of the huge concentration of microstructural defects present in these materials [8].

In ODS EUROFER, the behaviour of $\bar{\tau}$ and I_2 is reverse to that of M EUROFER, i.e. they continue increasing although the τ_2 values drop from 345 ps to 297 ps. These results in ODS EUROFER are interpreted as follows. ODS EUROFER has a much higher concentration of sites for the nucleation of stable Ar-decorated cavities than M-EUROFER due to the Y_2O_3 dispersion. The nanoparticles of this dispersion are very strong sink biased for inert gas atoms and vacancies, lowering the probability that vacancies and Ar-vacancy pairs released from unstable voids sink at the external surfaces of the sample. Now, if unstable voids and particle-stabilized cavities coexist in the stage 823–1323 K, the annealing out of the unstable voids for $T \geqslant 1323$ K should result in a decrease in I_2 as it occurs for M EUROFER, but the opposite effect is observed. This can occur if the positron trapping cross section of the stable cavities, which scales with their positron binding energy, increases due to the coarsening by entrapment of vacancies and Ar-vacancy pairs realised by unstable voids. According to the calculations for He and Kr in metals [25], positron binding energy to inert gas-decorated voids increase with increasing void size and their corresponding positron lifetimes result in shorter values than those for gas-free voids containing fewer vacancies. To attribute the I_2 increase to nucleation, and the growth of other new cavities may be ruled out because the stable cavities observed by TEM are associated to the particle dispersion that already appeared acting as effective positron traps in the initial stage, as the lifetime and CDB reflect.

5. Conclusions

Ar atoms absorbed during the MA process of EUROFER are active nucleant agents for vacancy clusters irrespective of the presence of particle dispersion in the material. However, particle dispersion appears to overstimulate cavity nucleation and stabilise them. Y_2O_3 particles and other unidentified particles, which may have precipitated during annealing, promote nucleation, coarsening and stabilization of the cavities in EUROFER produced by MA and HIP.

The positron annihilation experiments reveal that the Y_2O_3/matrix interfaces act as very strong and stable sinks for Ar and vacancies. Cavity coarsening starts at $\sim$800 K when first order Ar-vacancy clusters diffuse towards pre-existing voids, and the nucleation and the growth of new cavities appear to occur at $T \geqslant 1023$ K. Gas-free cavities and cavities not associated to particles annealed out for $T \geqslant 1323$ K, while those gas-decorated and associated to particles remained stable after annealing at 1523 K. TEM observations confirm this point. The present results point to these cavities as one of the causes of embrittlement and poor impact toughness of ODS EUROFER.

Acknowledgements

The Dirección General de Investigación of Spain, through grant MAT2004-1819, funded this work. The financial support from the Comunidad de Madrid, through the program ESTRUMAT-CM Grant S-0505/MAT/0077 is also gratefully acknowledged.

References

[1] S. Ukai, M. Harada, H. Okada, M. Inoue, S. Nomura, S. Shikakura, K. Asabe, T. Nishida, M. Fijiwara, J. Nucl. Mater. 204 (1993) 65–73.
[2] A. Hishinuma, A. Kohyama, R.L. Klueh, D.S. Gelles, W. Dietz, K. Ehrlich, J. Nucl. Mater. 258–263 (1998) 193–204.
[3] S. Ukai, M. Fujiwara, J. Nucl. Mater. 307–311 (2002) 749.
[4] S. Jitsukawa, A. Kimura, A. Kohyama, R.L. Klueh, A.A. Tavasoli, B. Van der Schaaf, G.R. Odette, J.W. Rensman, M. Victoria, C. Petersen, J. Nucl. Mater. 329–333 (2004) 39.
[5] R. Lindau, A. Möslang, M. Schirra, P. Schlossmacher, M. Klimenkov, J. Nucl. Mater. 307–311 (2002) 769.
[6] R. Schaublin, T. Leguey, P. Spätig, N. Baluc, M. Victoria, J. Nucl. Mater. 307–311 (2002) 778.
[7] R. Schaublin, A. Ramar, N. Baluc, V. de Castro, M.A. Monge, T. Leguey, N. Schmid, C. Bonjour, J. Nucl. Mater. 351 (2006) 247.
[8] V. de Castro, T. Leguey, A. Muñoz, M.A. Monge, P. Fernández, A.M. Lancha, R. Pareja, J. Nucl. Mater. 367–370 (2007) 196.
[9] M. Klimiankou, R. Lindau, A. Möslang, J. Nucl. Mater. 367–370 (2007) 173.
[10] Z. Oksiuta, N. Baluc, J. Nucl. Mater. (2007), doi:10.1016/j.nucmat.2007.08.004.
[11] N. Akasaka, S. Yamashita, T. Yoshitake, S. Ukai, A. Kimura, J. Nucl. Mater. 329–333 (2004) 1053.
[12] S. Yamashita, S. Watanabe, S. Ohnuki, H. Takahashi, N. Akasaka, S. Ukai, J. Nucl. Mater. 283–287 (2000) 647.
[13] A. Kimura, R. Sugano, Y. Matsushita, S. Ukai, J. Phys. Chem. Solid 66 (2005) 504.
[14] M. Klimiankou, R. Lindau, A. Möslang, Micron 36 (2005) 1.
[15] G. Brauer, L. Liszkay, B. Molnar, R. Krause, Nucl. Eng. Design 127 (1991) 47.
[16] V. Slugen, D. Segers, P.M.A. de Bakker, E. de Grave, V. Magula, T. van Hoecke, B. van Waeyenberge, J. Nucl. Mater. 274 (1999) 273.
[17] P. Asoka-Kumar, M. Alatalo, V.J. Ghosh, A.C. Kruseman, B. Nielsen, K.G. Lynn, Phys. Rev. Lett. 77 (1996) 2097.
[18] V. de Castro, T. Leguey, M.A. Monge, A. Muñoz, R. Pareja, D.R. Amador, J.M. Torralba, M. Victoria, J. Nucl. Mater. 322 (2003) 228.
[19] Y. Nagai, Z. Tang, M. Hasegawa, Rad. Phys. Chem. 58 (2000) 737.
[20] A. Vehanen, P. Hautojärvi, J. Johansson, J. Yli-Kaupila, P. Moser, Phys. Rev. B 25 (1982) 762.
[21] R. Pareja, N. de Diego, R.M. de la Cruz, J. del Río, Nucl. Tech. 104 (1993) 52.
[22] M.J. Puska, R.M. Nieminen, J. Phys. F: Met. Phys. 13 (1983) 333–346.
[23] P. Jena, B.K. Rao, Phys. Rev. B 31 (1985) 5634.
[24] M. Eldrup, J.H. Evans, J. Phys. F: Met. Phys. 12 (1982) 1265.
[25] K.O. Jensen, R.M. Nieminem, Phys. Rev. B 36 (1987) 8219.
[26] M.J. Puska, P. Lanki, R.M. Nieminen, J. Phys.: Condens. Matter 1 (1989) 6081–6094.